

A study on the formation and trend of the Brewer-Dobson circulation

K. Okamoto,¹ K. Sato,¹ and H. Akiyoshi²

Received 26 August 2010; revised 28 February 2011; accepted 4 March 2011; published 27 May 2011.

[1] The Brewer-Dobson circulation (BDC) is approximately expressed by the residual circulation (RC) and considered to be driven by the body force induced by the breaking and/or dissipation of atmospheric waves. The contribution of different types of waves to the RC in the Center for Climate System Research/National Institute for Environmental Studies (CCSR/NIES) Chemistry Climate Model (CCM) is diagnosed using the “downward control principle (DC).” Gravity wave drag (GWD) including orographic gravity wave drag (OGWD) has a great influence on the RC in the low and middle latitudes of the lower stratosphere. In particular, the summer hemispheric low-latitude part of winter circulation is mainly formed by the GWD. These results are consistent with the estimates of the GWD contribution using reanalysis data by subtracting the resolved wave contribution from the RC with DC principle. In addition, it is seen that the net upward mass flux on the 70 hPa surface is strengthened during the 21st century because of the upward shift of the OGWD, which is consistent with previous studies. These conclusions indicate that gravity waves play an important role in maintaining the BDC.

Citation: Okamoto, K., K. Sato, and H. Akiyoshi (2011), A study on the formation and trend of the Brewer-Dobson circulation, *J. Geophys. Res.*, 116, D10117, doi:10.1029/2010JD014953.

1. Introduction

[2] Stratospheric chemical tracer distributions are modified by the global-scale circulation consisting of an upwelling branch in the tropics and downwelling branches in the higher latitudes. This circulation is called the Brewer-Dobson circulation (BDC), named after its discoverers, Brewer and Dobson, who observed water vapor and ozone, respectively [Brewer, 1949; Dobson, 1952]. It is recognized that most stratospheric air comes from the troposphere passing through the tropical tropopause. This troposphere-stratosphere mass exchange controlled by the BDC is expressed as the net upward mass flux in the tropics, which is an index of the strength of the BDC [Holton, 1990]. The overturning time, which is defined as the mass of the atmosphere above 70 hPa (3.642×10^{17} kg) divided by the annual mean net upward mass flux, is expected to be about five years based on observations and model simulations [Rosenlof, 1995]. The residual circulation (RC) is a good approximation of the BDC [Andrews *et al.*, 1987], although the BDC is an overall stratospheric transport system including mixing processes as well. In this paper, a study regarding the BDC was made by focusing on the RC. The driving mechanism of the RC has been examined by some theoretical studies, and a well-known mechanism is “the downward control principle (DC)” proposed by Haynes *et al.* [1991]. According to this

mechanism, the meridional flow is driven by the wave forcing in the middle latitudes associated with the breaking and/or dissipation of the waves propagating from the troposphere. The vertical flows are then induced in higher and lower latitudes by mass conservation. Since there is a frictional forcing in the lower boundary of the atmosphere, a flow can violate the conservation law of the angular momentum at ground surface; thus, the stratospheric wave forcing can drive the circulation below, although the stratospheric portion of the near-ground return flow is minute. Previous studies suggest that the main driver of the RC is the wave forcing of planetary waves propagating into the middle stratosphere [Plumb, 2002; Shepherd, 2007]. They also suggest the importance of synoptic waves in the lower stratosphere and importance of the gravity waves in the mesosphere. In addition, it is known that gravity waves also influence the formation of the RC. In this study, the contribution of respective waves to the RC is examined in the meridional cross section using CCM data. In addition, similar analysis is performed using European Centre for Medium-Range Weather Forecasts Reanalysis-Interim (ERA-Interim) data, which observational data were assimilated into, to confirm the model results.

[3] Recent CCMs simulate future climate changes under the scenarios by IPCC regarding the increased rate of greenhouse gases (GHG) concentration and the scenarios by WMO regarding the increased rate of the concentrations of the ozone-depleting substances [Intergovernmental Panel on Climate Change (IPCC), 2000; World Meteorological Organization/United Nations Environment Program (WMO/UNEP), 2003, chapter 6]. The change of the RC, which modifies the distribution of various minor con-

¹Department of Earth and Planetary Physics, University of Tokyo, Tokyo, Japan.

²National Institute for Environmental Studies, Tsukuba, Japan.

stituents, is important for the ozone recovery owing to two possible reasons. The first is its transport ability, and the second is the adiabatic heating/cooling that influences the formation of the polar stratospheric cloud, and thus indirectly influences the ozone destruction through heterogeneous reaction on it. Most CCM simulations indicate a strengthening of the BDC [Butchart *et al.*, 2000, 2006; Garcia and Randel, 2008; McLandress and Shepherd, 2009]. It is generally expected that GHG increase modifies the radiative balance to cause warming in the troposphere and cooling in the stratosphere. The temperature fluctuation causes a change in the background wind field through the thermal wind balance, and hence leads to a change of the spatial distribution of the wave forcings [Garcia and Randel, 2008; McLandress and Shepherd, 2009]. McLandress and Shepherd [2009] showed an increase trend of the net upward mass flux at the 70 hPa surface in the 21st century using Canadian Middle Atmosphere Model (CMAM) data. They concluded that this increase is largely due to the upward shift of the orographic gravity wave drag (OGWD) to around 70 hPa. In this study, the change in the wave forcing distribution for interannual variability of the net upward mass flux is examined using the Center for Climate System Research/National Institute for Environmental Studies CCM (CCSR/NIES CCM) REF2 data providing a diagnosis using a different CCM to compare with the results obtained by McLandress and Shepherd [2009].

[4] The configuration of this paper is as follows. In section 2, we discuss the DC principle by Haynes *et al.* [1991] and derive several important formulas used in this study. Description of CCSR/NIES CCM and ERA-Interim data is made in section 3. In section 4, the DC theory is applied to evaluate the respective contribution of various waves, including planetary, synoptic and gravity waves, to the formation of the RC. A comparison of reanalysis data confirms the results. In section 5, we examine the trend of the RC in the 21st century in terms of the stream function and the net upward mass flux, particularly, the effects of gravity wave drag on the RC. Summary and concluding remarks are given in section 6.

2. The Downward Control Analysis

[5] The DC principle [Haynes *et al.*, 1991] is a useful theory for evaluating contributions of different types of wave drag to the residual mean circulation. This principle states that in the steady state, the extratropical meridional mass flow is controlled solely by the sum of all zonal forces above the pressure surface. Several important formulas are derived to show the DC principle for zonal mean fields in the steady condition in the transformed Eulerian mean (TEM) framework [Andrews *et al.*, 1987].

2.1. The Residual Circulation

[6] In the steady state, zonal momentum equation in log-pressure coordinates in the TEM system is written as

$$-\hat{f}\bar{v}^* = \frac{1}{\rho_0 a \cos \phi} \nabla \cdot \mathbf{F} + \bar{\mathbf{X}} = \bar{\mathcal{F}}, \quad (1) \quad \text{and}$$

$$\nabla \cdot \mathbf{F} = \frac{1}{a \cos \phi} \frac{\partial}{\partial \phi} (F_\phi \cos \phi) + \frac{\partial}{\partial z} F_z, \quad (2)$$

$$\mathbf{F} = \rho_0 a \cos \phi \left(\bar{u}_z \frac{\overline{v'\theta'}}{\bar{\theta}_z} - \overline{v'u'}, \hat{f} \frac{\overline{v'\theta'}}{\bar{\theta}_z} - \overline{w'u'} \right) \equiv (F_\phi, F_z), \quad (3)$$

where $\bar{\mathbf{X}}$ represents any unresolved zonal force (e.g., GWD); $\nabla \cdot \mathbf{F}$ is the divergence of the resolved Eliassen-Palm (E-P) flux (EPFD); \bar{v}^* and \bar{w}^* are the meridional and vertical components of the residual velocity, respectively; a is the radius of the Earth; ϕ is the latitude; \bar{u} is the zonal mean zonal wind; $f = 2\Omega \sin \phi$ is the Coriolis parameter where Ω is the rotation rate of the Earth; z is the log-pressure height; ρ_0 is the reference density of air; and $\hat{f} = f - (a \cos \phi)^{-1} \partial(\bar{u} \cos \phi) / \partial \phi$. In spherical coordinates the continuity equation is expressed as

$$\frac{1}{a \cos \phi} \frac{\partial}{\partial \phi} (\bar{v}^* \cos \phi) + \frac{1}{\rho_0} \frac{\partial}{\partial z} (\rho_0 \bar{w}^*) = 0. \quad (4)$$

Thus, a stream function for the residual velocities can be defined as

$$\bar{v}^* \equiv -\frac{1}{\rho_0 \cos \phi} \frac{\partial \Psi}{\partial z}, \quad \bar{w}^* \equiv \frac{1}{\rho_0 a \cos \phi} \frac{\partial \Psi}{\partial \phi}. \quad (5)$$

By substituting (5) into (1), integrating with respect to z , and rewriting in pressure coordinates we obtain

$$\Psi(\phi, p) = \frac{\cos \phi}{g} \int_p^0 \frac{\bar{\mathcal{F}}}{\hat{f}} dp', \quad (6)$$

where g is the gravitational acceleration. This equation is an important equation for the analysis of this paper. Equation (6) indicates that the strength and direction of the residual circulation at a given latitude ϕ and a pressure level p is expressed by the sum of all zonal forcings above the pressure level p at the latitude ϕ . The stream function is calculated so that the stream function at the top of atmosphere is 0.

[7] In this paper, a subscript to show “direct” is used for the result calculated by the TEM analysis using (5), that is, Ψ_{direct} . The subscripts “dc”, “gwd” and “epfd” are used to represent the contribution of the zonal forcing by all waves, parameterized gravity waves, and resolved waves, respectively, which are calculated by the DC analysis using (6), that is, Ψ_{dc} , Ψ_{gwd} , and Ψ_{epfd} .

2.2. The Vertical Mass Flux

[8] The net vertical mass flux is also an important quantity for the expression of the RC because it is equivalent to the troposphere-stratosphere mass exchange. Following Holton [1990], the area-averaged extratropical vertical mass fluxes across an isobaric surface in the northern hemisphere (NH) and southern hemisphere (SH), $F_{\text{direct}}^{\text{NH}}$ and $F_{\text{direct}}^{\text{SH}}$, are expressed as

$$F_{\text{direct}}^{\text{NH}} = 2\pi a^2 \rho_0 \int_{\phi_t^{\text{NH}}}^{\pi/2} \bar{w}_{\text{direct}}^* \cos \phi d\phi, \quad (7)$$

$$F_{\text{direct}}^{\text{SH}} = 2\pi a^2 \rho_0 \int_{-\pi/2}^{\phi_t^{\text{SH}}} \bar{w}_{\text{direct}}^* \cos \phi d\phi, \quad (8)$$

respectively. Here, ϕ_t^{NH} and ϕ_t^{SH} are the so-called turn-around latitudes (TLs) in the NH and SH, respectively, where tropical upwelling changes to extratropical downwelling; in other words, the latitudes at which the magnitude of the mass stream function Ψ_{direct} is maximized. Note that $F_{\text{direct}}^{\text{NH}}$ and $F_{\text{direct}}^{\text{SH}}$ provide the sum of the downward mass flux in respective hemispheres in the stratosphere because the sign of $\overline{w}_{\text{direct}}$ anywhere in the region between the TL and a pole is usually negative. As Ψ vanishes at the poles, the net downward mass fluxes in respective hemispheres are given using (5), by

$$F_{\text{direct}}^{\text{NH}} = -2\pi a \Psi_{\text{direct}}(\phi_t^{\text{NH}}) \quad (9)$$

$$F_{\text{direct}}^{\text{SH}} = 2\pi a \Psi_{\text{direct}}(\phi_t^{\text{SH}}). \quad (10)$$

Thus, $F_{\text{direct}}^{\text{NH}}$ and $F_{\text{direct}}^{\text{SH}}$ depend on stream function values only at TLs. From the constraint of zero global average mass flux, the net upward mass flux, which appears mainly in the tropics, is given by

$$F_{\text{direct}}^{\text{tr}} = -(F_{\text{direct}}^{\text{NH}} + F_{\text{direct}}^{\text{SH}}) = 2\pi a [\Psi_{\text{direct}}(\phi_t^{\text{NH}}) - \Psi_{\text{direct}}(\phi_t^{\text{SH}})]. \quad (11)$$

These mass fluxes can also be evaluated by the DC theory using Ψ_{dc} at the TLs. Note that the stream function at a TL depends only on the zonal force at the TL (see equation (6)).

3. Description of the Model and Data Set

[9] The CCSR/NIES CCM simulation whose data is used in this study was made as a part of Stratospheric Processes And their Role in Climate (SPARC) Chemistry-Climate Model Validation (CCMVal) research activity. The model includes a fully interactive stratospheric chemistry module, radiation scheme, and other parameterizations [Eyring *et al.*, 2006]. The model has 34 vertical layers in sigma coordinates at height intervals of one to a few kilometers with a top level at 0.012 hPa. The vertical resolution around the pressure level of 70 hPa, the focused level in this paper, is 1–2 km, which is comparable to that of *McLandress and Shepherd* [2009] around the level. The horizontal resolution is T42 (about $2.8^\circ \times 2.8^\circ$). Gravity wave parameterizations were used to include the effects of subgrid-scale gravity waves. *McFarlane's* [1987] scheme was applied as the orographic gravity wave parameterization, while the nonorographic gravity wave parameterization as presented by *Hines* [1997] was incorporated. Outputs from the REF2 run of the CCMVal that simulated the atmospheric fields in the 21st century were used in the present study. In the calculation, the time evolution scenario of the greenhouse gases such as the CO_2 , CH_4 , and N_2O concentrations at the surface was taken from the IPCC-A1B scenario [IPCC, 2000], and that of halogen gases was taken from the WMO-Ab scenario [WMO/UNEP, 2003], not including the effects of the quasi-biennial oscillation (QBO), the 11 year solar cycle, and volcanic eruptions. The monthly mean sea surface temperature data were provided from the 20th century simulation with an atmosphere–ocean coupled general circulation model (CGCM). The CGCM is called MIROC and was developed by CCSR, NIES, and the Frontier Research Center for Global

Change (FRCGC). This model data is useful for examining the present and future stratospheric climate because this model well reproduces dynamical fields and reasonable future ozone change, although severe cold bias is observed in the tropical tropopause and southern polar region compared with the other models in CCMVal [Eyring *et al.*, 2006; Butchart *et al.*, 2010]. See *Akiyoshi et al.* [2009, 2010] for more details of this model description. Physical quantities are interpolated to 31 vertical layers with a top level of 0.1 hPa in isobaric coordinates to ease analysis.

[10] Analyses for the time period 2000–2008 are performed as the “present1” climate in section 4. In section 5, the “present2” and “future” climates refers to the time periods of 1995–2010 (including the “present1” climate) and 2065–2080, respectively. The analyses on long-term climate change were made by comparing the present2 and future climates in section 5. Linear trends are estimated for the time period of 2005–2070 for various parameters.

[11] The performance of the CCSR/NIES CCM is evaluated by comparison with the ERA-Interim data. Physical parameters in ERA-Interim data used in this study are smoothed to lower the horizontal resolution to $3^\circ \times 3^\circ$, which is comparable to that of CCSR/NIES CCM. Figure 1 shows the zonal mean zonal wind calculated from the CCM data and from ERA-Interim data in the NH winter months, December–February (DJF), for the present1 climate. The strength and positions of the tropospheric and stratospheric jets are well reproduced by the CCM; for instance, subtropical jets in the NH are located around a latitude of 30° and around 200 hPa with a magnitude of about 40 m s^{-1} . This assures that the results on the RC obtained by the analysis using the CCM are realistic, although the polar night jet in the NH is slightly stronger in CCM data than in ERA-Interim data. Note that the jet structure plays an important role in the propagation and dissipation of both resolved and parameterized waves.

4. The Contribution of Wave Forcing to the BDC

[12] In this section, validity of the DC analysis is first confirmed by comparing Ψ_{dc} and Ψ_{direct} in the meridional cross section. Next, the contributions of respective waves to the formation of RC are separately examined using the CCM data. The effect of gravity wave drag is estimated for ERA-Interim data through the DC theory and comparing it with the CCM results. Finally in this section, the net upward mass flux is examined in terms of seasonal variation and contribution of each wave drag.

4.1. Results From the CCM Data Analysis and Validation of the DC Analysis

[13] Figure 2 shows the meridional cross sections of mass stream function obtained by the DC analysis and direct calculation for the present1 climate in DJF when the RC is strongest. The DC analysis is considered to be appropriate only for solstice seasons because a steady state condition is assumed. The DC analysis is also not available for the tropics because of \hat{f} in the denominator of equation (6). Thus, Figures 2a and 2c–2h show the results only in the latitudes higher than 10° .

[14] It is clear that Ψ_{dc} , the sum of Ψ_{epfd} and Ψ_{gwd} , is in good agreement with Ψ_{direct} in terms of strength and loca-

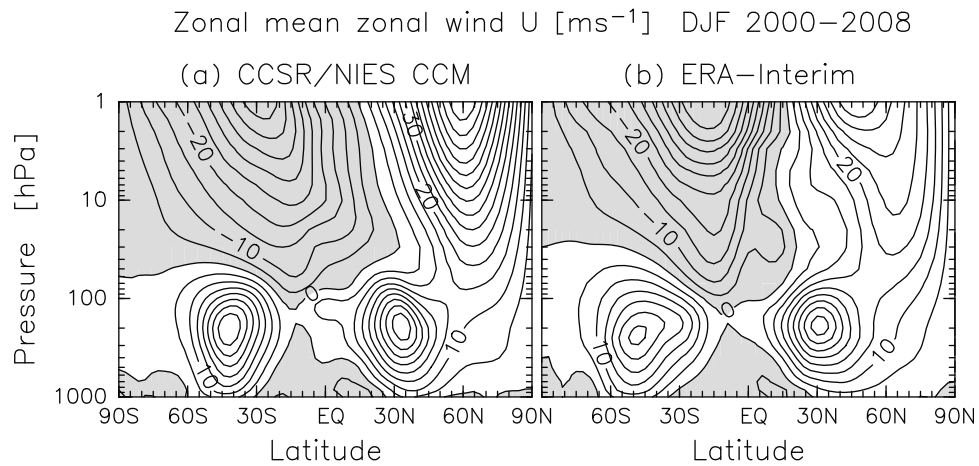


Figure 1. Meridional cross sections of zonal mean zonal wind (\bar{u}) during NH winter (DJF) for (a) CCSR/NIES CCM and (b) ERA-Interim for the period 2000–2008. Contour interval is 5 m s^{-1} . Eastlies are shaded.

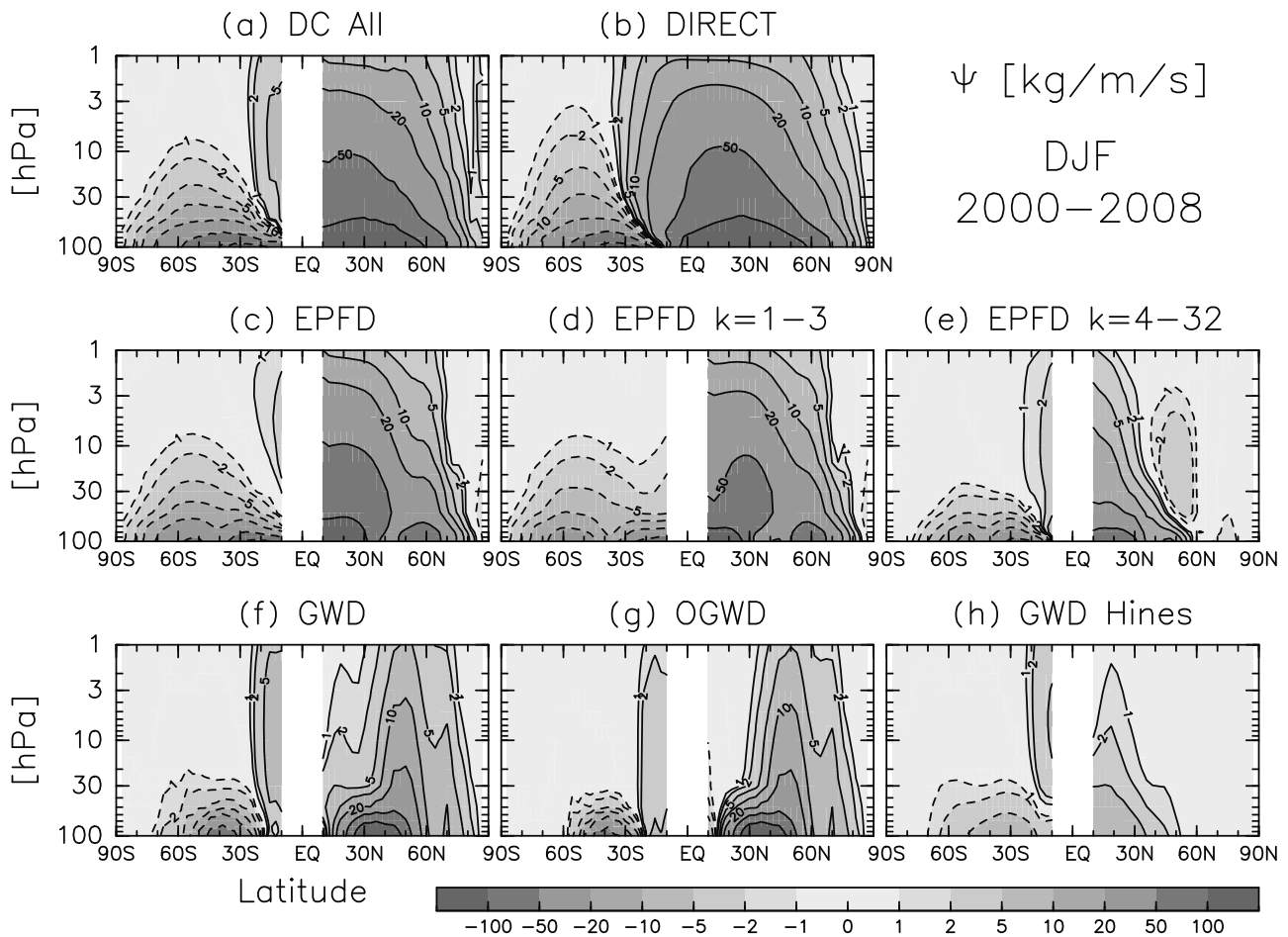


Figure 2. Meridional cross sections of the mass stream function in DJF for the present1 climate (2000–2008) calculated from CCM data by (b) the direct method and by the DC theory using drag from (a) all waves, (c) resolved waves (EPFD), resolved waves with zonal wave numbers of (d) 1–3 ($k = 1-3$), and (e) $k = 4-32$, (f) all parameterized gravity waves (GWD: Figures 2g + 2h), (g) parameterized orographic gravity waves (OGWD), and (h) parameterized nonstationary gravity waves (GWD Hines). Units are $\text{kg m}^{-1} \text{ s}^{-1}$.

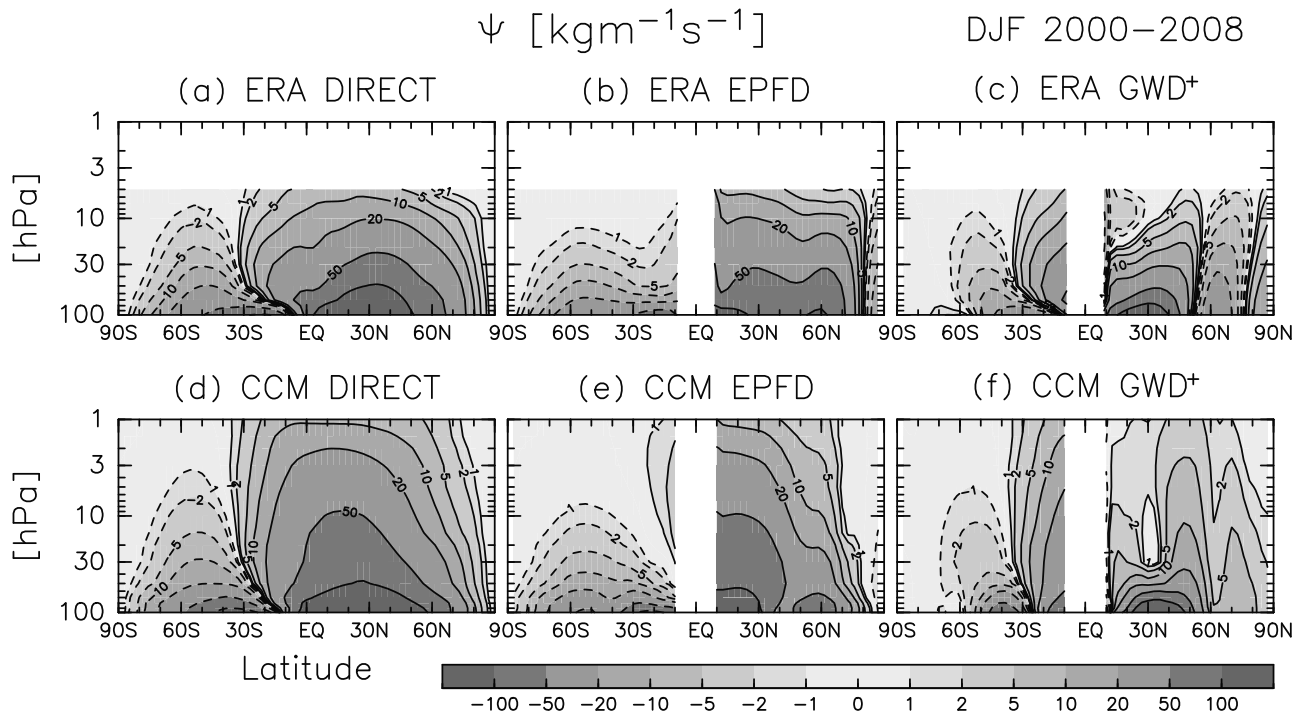


Figure 3. Same as Figure 2 but for the result using (a, b, and c) ERA-Interim data and (d, e, and f) CCM data. $\Psi_{\text{gwd}\uparrow}$ (Figures 3c and 3f) are estimated as the difference between Ψ_{direct} (Figures 3a and 3d) and Ψ_{epfd} (Figures 3b and 3e).

tion. This good quantitative agreement between Ψ_{dc} and Ψ_{direct} assures that the DC analysis provides accurate estimates of the RC in the stratosphere. Thus, further analysis is made for the contribution of each kind of wave force to the RC.

[15] Overall structure of the RC is primarily determined by the resolved waves, especially planetary waves [Plumb, 2002] in the NH except for the middle latitudes, which is consistent with the result of *McLandress and Shepherd* [2009]. The NH cell of Ψ_{direct} extends much higher into the stratosphere compared with that of the SH mainly as a result of significant differences in the planetary wave drag between the two hemispheres as indicated by Figure 2d. The planetary waves hardly propagate into the stratosphere in the summer hemisphere where the easterly is dominant. The effects of synoptic wave drag are confined to the low latitudes and midlatitudes of the NH and do not extend deep into the stratosphere in the midlatitudes and high latitudes (Figure 2e). The circulation induced by OGWD is confined mainly to the middle latitudes in the NH (Figure 2g). The OGWD-induced and EPFD-induced circulations are comparable in the middle latitudes around 35°N in the lower stratosphere (below 50 hPa). The effect of nonstationary-GWD (GWD Hines) is generally small, though it is significant in the subtropics (Figure 2h).

[16] Another interesting point obtained in Figure 2 is that GWD-induced circulation is dominant in the summer hemisphere upwelling part (about 20°S) of the winter hemisphere cell (Figure 2f). This fact suggests that the GWD plays an important role for the extension of the winter cell to the summer hemisphere. This feature is not reported in previous studies.

4.2. The Estimation of GWD Contribution Using Reanalysis Data

[17] The validity of the results from the CCM data analysis is confirmed using ERA-Interim data. The stream function of RC is calculated directly as Ψ_{direct} and the contribution of the E-P flux divergence, Ψ_{epfd} , is calculated by using the DC theory. As Ψ_{direct} includes the effects of all waves in the atmosphere, GWD-induced circulation $\Psi_{\text{gwd}\uparrow}$ can be estimated by subtracting Ψ_{epfd} from Ψ_{direct} , that is,

$$\Psi_{\text{gwd}\uparrow} = \Psi_{\text{direct}} - \Psi_{\text{epfd}}. \quad (12)$$

Such estimates are possible in the steady state because the DC theory indicates that the mass stream function, the residual velocity, and the mass flux are all linear as to the wave forcing \mathcal{F} .

[18] Figure 3 shows the mass stream functions calculated by the direct method (Figures 3a and 3d), by the DC theory for resolved wave forcing (Figures 3b and 3e), and indirectly for gravity waves (Figures 3c and 3f) for DJF in the present1 climate from ERA-Interim data and CCM data, respectively. The RC estimated from ERA-Interim data (Figure 3a) consists of two-celled circulation, and is stronger in the NH than in the SH, which is in accord with the CCM result (Figure 3d).

[19] The calculation of Ψ at a given pressure level is performed by integrating \bar{v}^* (equation (5)), or by integrating wave drag (equation (6)) from the pressure to the top of atmosphere (0 hPa). Thus, the circulation in the upper stratosphere over 5 hPa is not obtained because of a lack of ERA-Interim data. The higher part of Ψ is, therefore, more

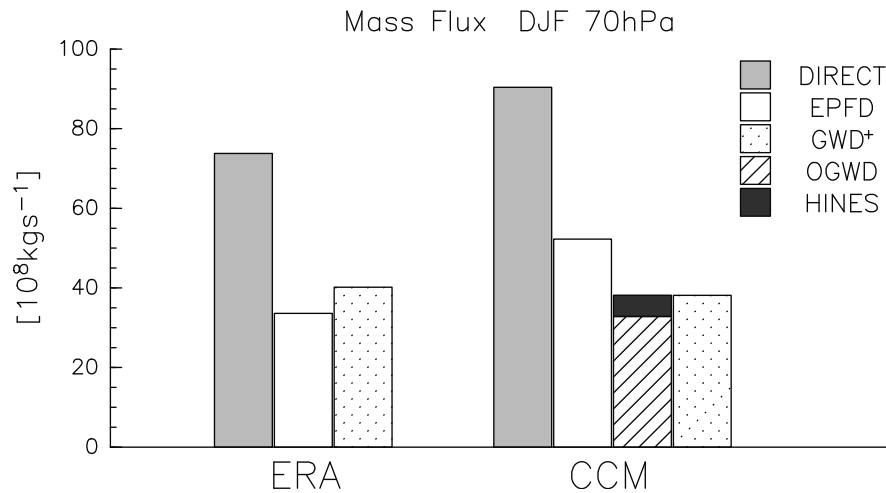


Figure 4. Contribution of each wave forcing to the net upward mass flux for DJF for the present1 climate (2000–2008).

largely affected by the missing of the data; hence, the difference observed in the upper stratosphere between the CCM and ERA-Interim should not be overinterpreted. In addition, $\Psi_{\text{gwd}\dagger}$ in CCM (Figure 3f) and $\Psi_{\text{gwd}\dagger}$ in ERA-Interim (Figure 3c) are different in some regions. There are a few possible explanations: forcings other than GWD, assumption of a steady state, and interannual variabilities in these regions. This point is, however, beyond the scope of this paper.

[20] However, the overall RC characteristics in the ERA-Interim data in the lower stratosphere are similar to the CCM results, assuring the validity of the results from the CCM data analysis: The resolved wave drag is a main component in determining the overall structure of the RC, though there are some differences in the planetary wave activity between the CCM and ERA-Interim results: for example, the planetary wave activity in the lower stratosphere is stronger in low latitudes and weaker in high latitudes for the CCM results (Figures 3b and 3e). The GWD considerably influences the RC in the lower stratosphere. It is of interest that $\Psi_{\text{gwd}\dagger}$ is dominant in the summer hemispheric upwelling branch of the winter RC cell, which is also consistent with the CCM results as noted above. In other words, it is suggested that the winter circulation of RC can extend to the summer hemisphere by the existence of the GWD.

4.3. The Wave Forcing Role in the Net Upward Mass Flux

[21] Contributions of zonal wave forcings to the net upward mass flux at 70 hPa in DJF for the present1 climate using CCM and ERA-Interim data are summarized in Figure 4. The contribution of GWD is as large as that of EPFD in ERA-Interim data. Thus, GWD and EPFD are essential to the mass circulation in the lower stratosphere. Figure 4 also shows the indirect estimation of the contribution of GWD at 70 hPa using CCM data. The value agrees with the sum of those of parameterized OGWD and nonographic GWD using CCM data within 0.1%. This result suggests that the DC analysis can be applied in DJF, and can be used for

accurate evaluation of the contribution of GWD using ERA-Interim data.

5. The Trend of the BDC

[22] In this section, possible changes of the RC in the 21st century are examined using projection data from the CCM REF2 run. Linear trends in the time period 2005–2070 of the residual mass stream function are calculated and discussed. The long-term variation of the contributions of respective wave forcings to the net upward mass flux is shown.

5.1. Linear Trend of the BDC

[23] Figure 5 shows linear trend of the seasonal mean mass stream function for DJF calculated by the direct method and by the DC theory for each wave force contribution. The NH cell in the lower stratosphere and a subtropical part of the SH cell in the lower stratosphere are intensified. The trend of the annual mean residual circulation Ψ_{direct} consists of two cells with the same sign as the present1 climate except for the Antarctic region, indicating strengthening of the residual circulation at most heights. This feature is consistent with the results from the other CCM runs [Butchart *et al.*, 2006; McLandress and Shepherd, 2009].

[24] Similarity of Ψ_{direct} (Figure 5b) and Ψ_{dc} (Figure 5a) except for the NH subtropics around 10 hPa assures the validity of the DC analysis for trends. In the lower stratosphere, the trend of the circulation driven by the resolved wave drag (Figure 5c) consists of two or three cells in the NH. It is also seen by comparing Figures 5d and 5e that planetary waves are the most important among the resolved waves. The trend by OGWD has a positive cell in the middle latitudes of the NH. This positive cell by OGWD is stronger than the negative cell by EPFD, resulting in one-celled circulation in the NH lower stratosphere. Therefore, OGWD is important for strengthening the trend of the RC. In addition, the positive peak of the OGWD trend in the lower stratosphere significantly affects the net upward mass flux trend because the mass flux is determined only by the

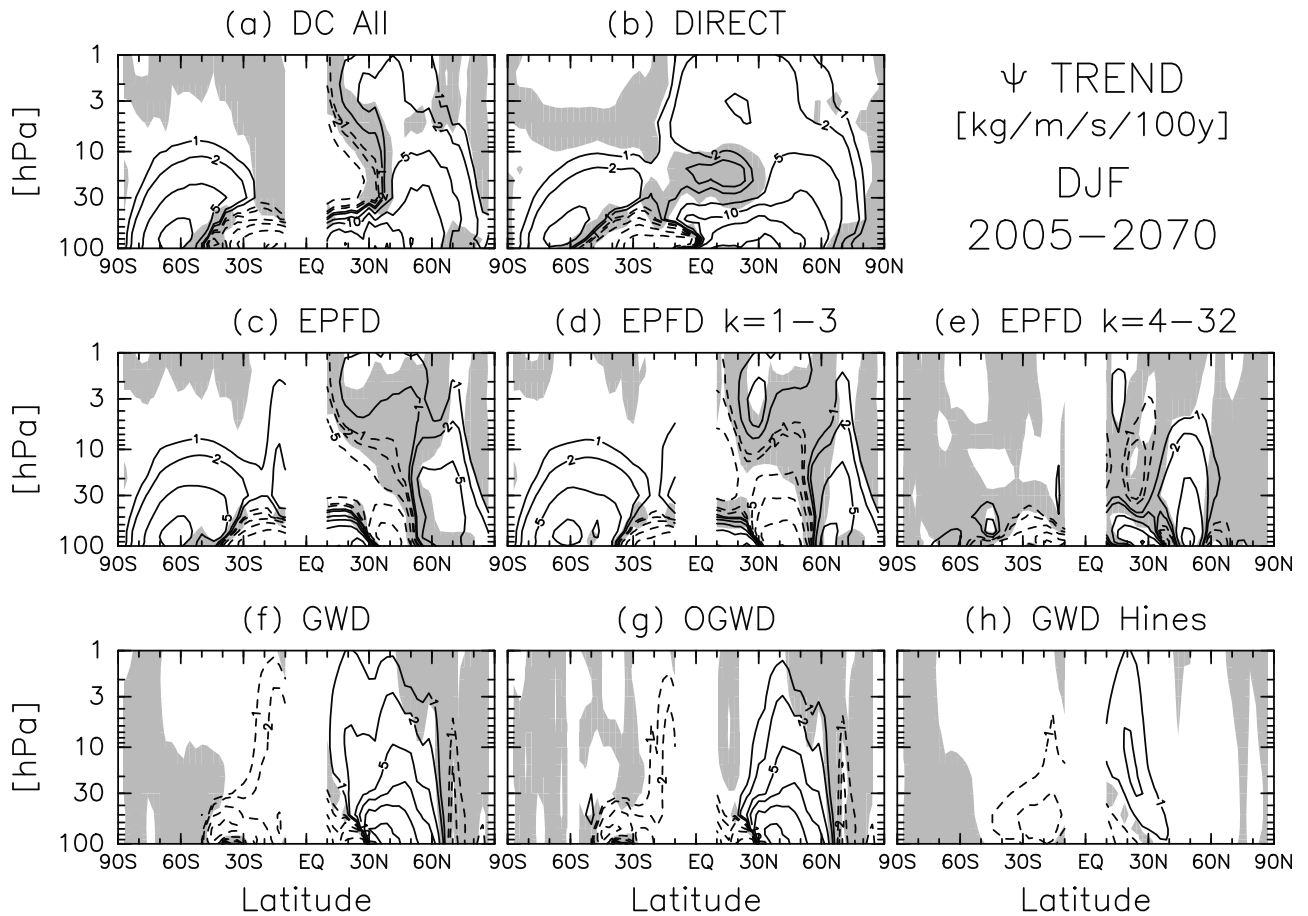


Figure 5. Same as Figure 2 but for linear trend of the mean stream function in DJF in the time period 2005–2070. Dark shading denotes the under 80% confidence levels.

stream function at the TL around 30° (see equation (11) and section 5.2). Synoptic wave drag effects are confined to low latitudes of the lower stratosphere and in middle latitudes of the middle stratosphere (Figure 5e). The circulation induced by nonstationary gravity waves has weak but intensifying trend, particularly, for low latitudes of the middle stratosphere in both the hemispheres (Figure 5h).

[25] In section 4, the importance of GWD for the winter circulation extending to the summer hemisphere was denoted. In spite of the positive trend of the RC in the summer hemispheric subtropics of the middle stratosphere (Figure 5b), the trend of stream function estimated by the downward control analysis is unclear due to insignificance (Figure 5a).

5.2. Long-Term Change of the Net Upward Mass Flux

[26] Figure 6a shows time series of the net upward mass flux at 70 hPa for DJF. The net upward mass flux has a strong seasonal cycle with a maximum in DJF [Rosenlof, 1995]. The net upward mass flux $F_{\text{direct}}^{\text{tr}}$ shows a nearly linear trend in each season, which agrees with the increased trend of RC in the tropics and the results of Butchart *et al.* [2006], Garcia and Randel [2008], and McLandress and Shepherd [2009]. The colored curves in Figure 6 denote the contributions of different types of wave drag to the net upward mass flux obtained from the DC analysis for DJF. Although the resolved wave drag (blue) accounts for more than half of the upward mass flux for solstice seasons in the

past climate, the trend of the upward mass flux by OGWD (pink) is comparable to and/or greater than that by the planetary wave drag. These results are consistent with those of McLandress and Shepherd [2009] using the CMAM. To examine the contribution of each hemisphere to the net upward mass flux, the downward mass flux is shown separately for the NH and SH in DJF in Figures 6b and 6c. The net downward mass flux is larger in the northern (winter) hemisphere for DJF during the entire period of 1978–2100 than in the southern (summer) hemisphere. Positive trends are seen for the net downward mass flux in all panels of Figure 6. The contribution of planetary wave drag (green) is dominant for the mass fluxes in the winter hemispheres. However, the trend of the contribution of the OGWD (pink) is largest for both hemispheres. The contribution of OGWD to the mass flux becomes comparable to that of the EPFD (blue) in the late 21st century. This result is different from that of McLandress and Shepherd [2009]; in their results, OGWD contribution is smaller than EPFD contribution throughout the 21st century. The magnitude of peaks of OGWD around 30°N in CCSR/NIES is about $2 \text{ m s}^{-1} \text{ d}^{-1}$ (see Figure 7), which is similar to the settings by McFarlane [1987] or Palmer *et al.* [1986].

5.3. The OGWD Trend Mechanism

[27] In this section, we will examine the change in the OGWD effect during the 21st century. According to the DC

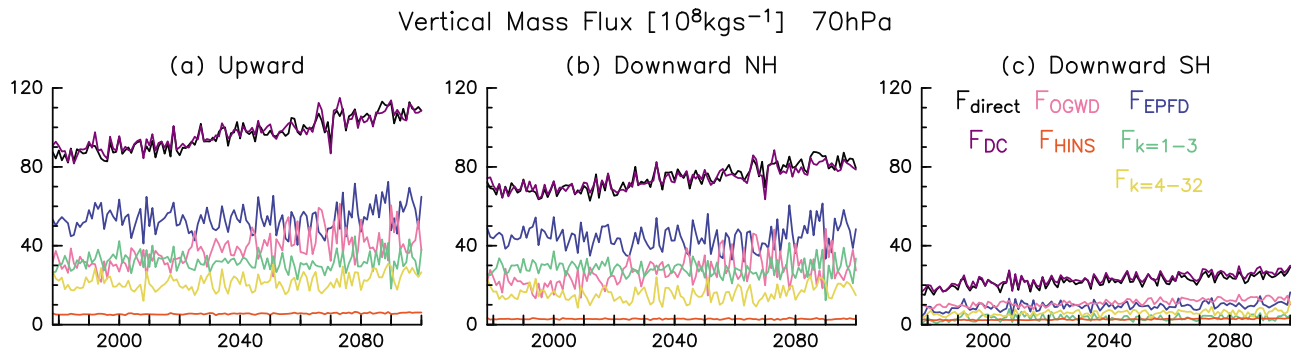


Figure 6. Time series of DJF mean net vertical mass flux at 70 hPa in (a) tropics (F^{tr}), (b) NH (F^{NH}), and (c) SH (F^{SH}). Direct calculation (black), DC estimations using OGWD (pink), EPFD (blue), planetary wave drag (green), synoptic wave drag (yellow), nonorographic gravity wave drag (red), and all wave forcing (purple) are displayed in each panel.

theory, the stream function of the residual circulation at a given pressure level is not influenced by the wave drag below the pressure level (equation (6)). Moreover, the net upward mass flux and its trend that are defined at 70 hPa depend on the sum of wave drag only at TLs (see equations (6) and (11)). The vertical distributions of EPFD and OGWD around 30°N in DJF are shown in Figure 7. The focused latitude 30°N is given by the TL at the 70 hPa surface in the NH. The difference between the future and present2 climate is responsible for the trend of the net upward mass flux. The OGWD in the height range between 70 hPa and 30 hPa in the future climate is significantly large, 1.25–2.73 times of magnitude than that in the present2 climate, while the difference in EPFD over 70 hPa is not remarkable. These differences are consistent with the increasing trend of the OGWD-induced mass flux and unremarkable trend of the EPFD-induced mass flux in DJF (Figure 6).

[28] Two possible mechanisms are considered for determining the change of OGWD. One is the change in the source momentum flux, and the other is the change in the distribution of the region in which the wave breaks in the meridional cross section. The latter would be reconfirmation of the result by *McLandress and Shepherd* [2009]. In CCM, the effects of the orographic gravity waves are included using the parameterization scheme developed by *McFarlane* [1987]. Orographic gravity waves are excited in a stably stratified air flowing over irregular terrain. Such waves may propagate freely to considerable altitudes before being significantly dissipated or absorbed. The wave drag parameterization developed by *McFarlane* is based on simple linear theory: The momentum flux divergence occurs in association with the breaking of the stationary monochromatic gravity waves, in which the wave breaking is expressed by the wave saturation hypothesis as proposed by *Lindzen* [1981].

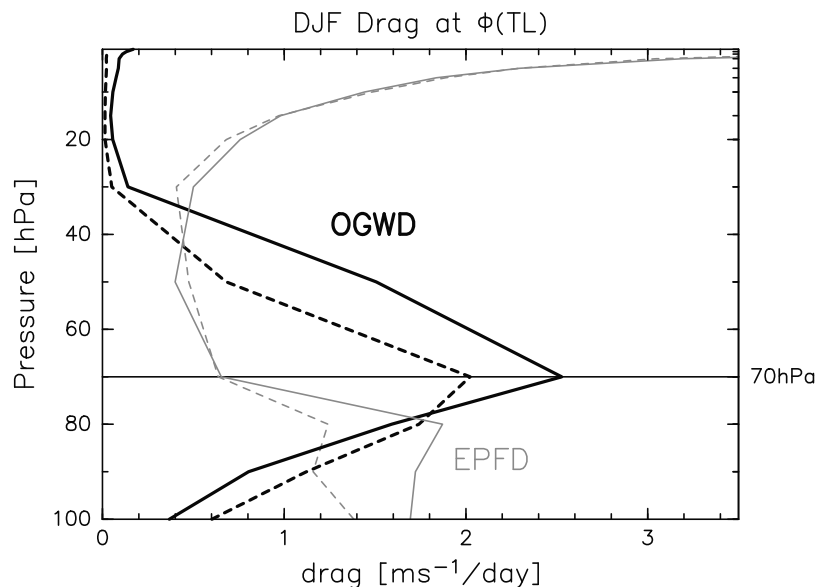


Figure 7. Vertical profiles of EPFD and OGWD at a TL in NH in DJF. The TL is estimated at 70 hPa (about 30°N). Solid lines are results for the future (2065–2080), and dashed lines for the present2 (1995–2010). The horizontal line shows the height of 70 hPa.

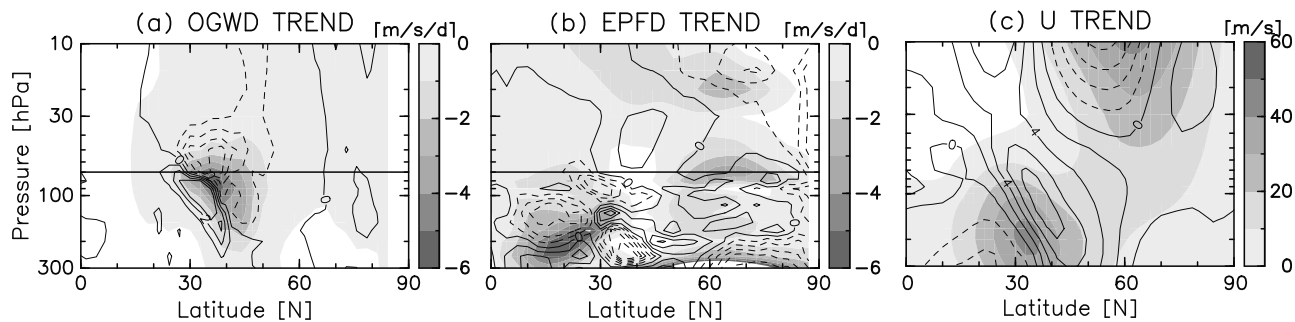


Figure 8. Meridional cross sections of zonal mean of (a) OGWD, (b) EPFD, and (c) zonal wind in DJF for the present2 (shadings) and their trends (contours). Contour intervals are (a and b) $0.4 \text{ m s}^{-1}/100$ year and (c) $2 \text{ m s}^{-1}/100$ year. The horizontal lines in Figures 8a and 8b show the height of 70 hPa.

[29] The source momentum flux of the orographic gravity wave at the ground, τ , is approximately expressed by McFarlane’s parameterization

$$\tau \approx \frac{\mu h^2}{2} \rho_0 N_0 U_0, \quad (13)$$

where μ is the wave number; h is the amplitude of the orographic perturbation; ρ_0 is the air density at the ground surface; N_0 is the Brunt-Väisälä frequency at the ground surface; and U_0 is the magnitude of the horizontal surface wind.

[30] The source momentum flux is reproduced using equation (13) since the data was not saved. The difference in the source momentum flux of the orographic gravity waves at the surface between the future and present2 climate is less than 5% (not shown). This fact suggests that the source intensity of orographic gravity wave is not the main factor to modify the effect of OGWD in the trend of the residual circulation in the lower stratosphere.

[31] Another important mechanism determining the OGWD is wave breaking, which occurs when the amplitude of horizontal wind fluctuations associated with the orographic gravity wave exceeds the mean wind and when the vertical structure of temperature gets unstable. In such situations, the OGWD parameterization adjusts τ to a critical value so as to make the static stability neutral. This is the wave saturation hypothesis [Lindzen, 1981]. The OGWD is then obtained as convergence of τ ,

$$\frac{\partial U}{\partial t} = g \frac{\partial \tau}{\partial p}. \quad (14)$$

The breaking of orographic gravity wave tends to occur more easily when the mean wind is weaker. Thus, the peak of OGWD is located in the weak wind region above the subtropical jet core. See McFarlane [1987] for detailed discussion.

[32] The trends of OGWD, EPFD, and zonal mean zonal wind in the meridional cross section of the upper troposphere and lower stratosphere for the NH are shown in Figure 8 by contours. Shadings show respective quantities for the present2 climate. As observed, there is no significant peak for EPFD near the TL (around 30°) above 70 hPa in the present2 climate and its trend. Instead, the influence of EPFD is larger for the trend of the stream function in the

high latitudes because of the increasing trend of EPFD in the higher latitudes and altitudes (Figures 5c and 5d). In contrast, the peak of OGWD for the present2 climate is located in the middle latitudes near 70 hPa. A negative trend, such as an increase in wave drag, is observed above and slightly poleward of the present2 peak, and a positive trend, such as a decrease in wave drag, is located below and slightly equatorward of the present2 peak. These features indicate that the peak of OGWD has shifted upward from the present2. Thus, this upward shift of the OGWD peak around the TL seems imperative to increase the sum of OGWD above 70 hPa at the TL. Note that the change of TL at 70 hPa is not large; the difference between the present2 and future climate is smaller than 2° (not shown).

[33] The upward shift in OGWD is related to the trend of the subtropical jet, which becomes stronger and its peak altitude gets higher in the future (Figure 8c). This trend of the subtropical jet is attributable to the trend of temperature field caused by an increased CO_2 , because these trends obey the thermal wind balance. As CO_2 increases, the vertical profile of the temperature may change. In particular, the temperature increases in the troposphere and decreases in the stratosphere because of increased absorption (release) of infrared radiation in the troposphere (the stratosphere), resulting in the upward shift of the minimum temperature corresponding to the tropopause height [Son *et al.*, 2009]. Thus, the subtropical jet core shifts upward.

[34] Similar discussion on the change in the OGWD distribution associated with GHG increase was made by McLandress and Shepherd [2009] and shortly noted by Garcia and Randel [2008].

6. Summary and Concluding Remarks

[35] The stratospheric circulations for the present1 climate and its change in the 21st century are examined in terms of the stream function and the net vertical mass fluxes are examined using CCSR/NIES CCM REF2 data. The RC for the present1 climate is also analyzed using ERA-Interim data for the model validation.

[36] We initially examined the contribution of various kinds of waves to the RC for the present1 climate (2000–2008) based on the DC analysis. We found that planetary waves contribute mainly in the midstratosphere and upper stratosphere, especially above 30 hPa and in the high latitudes. The effect of synoptic-scale waves is confined in the

low latitudes and midlatitudes in the lower stratosphere. In the middle latitudes, the contribution of gravity waves is comparable to that of the planetary waves. These results are consistent with previous studies using different CCMs [McLandress and Shepherd, 2009]. In this study, it is also shown that the GWD including parameterized OGWD [McFarlane, 1987] and nonstationary GWD [Hines, 1997] significantly influence the formation of the summer hemispheric upward branch of the winter circulation in DJF. This factor was not previously reported. The GWD-induced circulation in the real atmosphere can be evaluated by subtracting Ψ_{epfd} from Ψ_{direct} using ERA-Interim data because reanalysis data are based on observation and include latently the effects of the GWD. The resultant $\Psi_{\text{gwd}\dagger}$ is in good agreement with the CCM data in terms of the importance of GWD in the middle latitudes of the lower stratosphere and the summer hemispheric subtropics. Therefore, it is concluded that the GWD in the lower stratosphere is crucial in the BDC formation.

[37] We then examined the trends of the RC in the 21st century. The mass stream functions in the CCM have increasing trend in the period 2005–2070, which is consistent with many previous studies using CCMs. We evaluated the trend of the contributions of wave drag to the RC in DJF. In the lower stratosphere, the trend of Ψ_{epfd} consists of two or three cells in the NH, while the Ψ_{gwd} has a large and positive cell in the middle latitudes. As a result, the trend of the lower stratospheric circulation in the NH is one-celled; the RC in the 21st century can be accelerated in all latitudes by combining various types of waves.

[38] The net upward mass flux, which is determined only by the stream function at the TL, has an increasing trend in all seasons, which is similar to the stream function. We examined the contribution of respective wave forcings to the trend of the net upward mass flux in DJF. The trend of the OGWD significantly influences the trend of the net upward mass flux in DJF, while the trend of EPFD-induced mass flux is not remarkable, although the trend of EPFD is also large for the net mass flux trend for the CMAM [McLandress and Shepherd, 2009]. Thus, the contribution of the OGWD to the BDC acceleration is comparable to or greater than that of the EPFD in the late 21st century.

[39] The trend of the net upward mass flux in DJF was largely attributed to that of OGWD at the TL in the NH. The mechanism of the change of OGWD is explored in detail. The difference in the source momentum mass flux of OGW between the future and present2 climate was small. In contrast, the OGWD above the 70 hPa at TL significantly increased and was attributed to the upward shift of the subtropical jet associated with upward shift of the tropopause in response to the increasing GHGs under the scenarios of IPCC [2000] in the 21st century. This mechanism is consistent with the work of McLandress and Shepherd [2009] and Garcia and Randel [2008].

[40] In this paper, we examined the contribution of various waves to the residual circulation using the DC theory. However, it may be difficult to apply the DC analysis for the equinox seasons where the assumption of steady state may not be valid; more generalized theory is necessary to investigate the seasonal variability of the BDC. For the future works, it is interesting to examine the interannual and seasonal variability in BDC using reanalysis data. Recent

observational studies do not indicate an acceleration of the BDC [Engel *et al.*, 2009]. As noted, most CCMs including the present model simulated the acceleration of the BDC. The BDC should closely be analyzed in terms of the RC together with mixing to clarify the mechanism. In addition, with respect to the DC principle, it is also important to investigate the RC in the mesosphere, focusing on the connection between the stratosphere and mesosphere.

[41] **Acknowledgments.** The authors thank Diane Pendlebury and Elisa Manzini for their useful comments and discussions. We also thank Tatsuya Nagashima and Yosuke Yamashita for providing codes of the orographic gravity wave parameterization scheme. ERA-Interim data were used for the analysis. Yoshihiro Tomikawa and Kazue Suzuki helped in the treatment. All figures in this paper are drawn by using the DCL library. This study is supported by Grant-in-Aid for Scientific Research (B) 22340134 of the Ministry of Education, Culture, Sports and Technology (MEXT), Japan, and by the Global Environmental Research Fund (GERF) of the Ministry of the Environment (MOE) of Japan (A-071), and the simulations were completed with the supercomputer at CGER of the National Institute for Environmental Studies (NIES).

References

- Akiyoshi, H., L. B. Zhou, Y. Yamashita, K. Sakamoto, M. Yoshiki, T. Nagashima, M. Takahashi, J. Kurokawa, M. Takigawa, and T. Imamura (2009), A CCM simulation of the breakup of the Antarctic polar vortex in the years 1980–2004 under the CCMVal scenarios, *J. Geophys. Res.*, *114*, D03103, doi:10.1029/2007JD009261.
- Akiyoshi, H., Y. Yamashita, K. Sakamoto, L. B. Zhou, and T. Imamura (2010), Recovery of stratospheric ozone in calculations by the Center for Climate System Research/National Institute for Environmental Studies chemistry-climate model under the CCMVal-REF2 scenario and a no-climate-change run, *J. Geophys. Res.*, *115*, D19301, doi:10.1029/2009JD012683.
- Andrews, D. G., J. R. Holton, and C. B. Leovy (1987), *Middle Atmosphere Dynamics*, 504 pp., Academic, San Diego, Calif.
- Brewer, A. W. (1949), Evidence for a world circulation provided by the measurements of helium and water vapour distribution in the stratosphere, *Q. J. R. Meteorol. Soc.*, *75*, 351–363.
- Butchart, N., J. Austin, J. R. Knight, A. A. Scaife, and M. L. Gallani (2000), The response of the stratospheric climate to projected changes in the concentrations of well-mixed greenhouse gases from 1992 to 2051, *J. Clim.*, *13*, 2142–2159.
- Butchart, N., et al. (2006), Simulations of anthropogenic change in the strength of the Brewer–Dobson circulation, *Clim. Dyn.*, *27*, 727–741, doi:10.1007/s00382-006-0162-4.
- Butchart, N., et al. (2010), Chemistry-climate model simulations of twenty-first century stratospheric climate and circulation changes, *J. Clim.*, *23*, 5349–5374, doi:10.1175/2010JCLI3404.1.
- Dobson, G. M. B. (1952), Ozone in the Earth's atmosphere, *Endeavour*, *11*, 215–219.
- Engel, A., et al. (2009), Age of stratospheric air unchanged within uncertainties over the past 30 years, *Nat. Geosci.*, *2*, 28–31, doi:10.1038/NNGEO388.
- Eyring, V., et al. (2006), Assessment of temperature, trace species, and ozone in chemistry-climate model simulations of the recent past, *J. Geophys. Res.*, *111*, D22308, doi:10.1029/2006JD007327.
- Garcia, R. R., and W. J. Randel (2008), Acceleration of the Brewer–Dobson circulation due to increases in greenhouse gases, *J. Atmos. Sci.*, *65*, 2731–2739, doi:10.1175/2008JAS2712.1.
- Haynes, P. H., C. J. Marks, M. E. McIntyre, T. G. Shepherd, and K. P. Shine (1991), On the “downward control” of extratropical diabatic circulations by eddy-induced mean zonal forces, *J. Atmos. Sci.*, *48*, 651–678.
- Hines, C. P. (1997), Doppler-spread parameterization of gravity-wave momentum deposition in the middle atmosphere. Part 2: Broad and quasi monochromatic spectra, and implementation, *J. Atmos. Sol. Terr. Phys.*, *59*, 387–400.
- Holton, J. R. (1990), On the global exchange of mass between the stratosphere and troposphere, *J. Atmos. Sci.*, *47*, 392–395.
- Intergovernmental Panel on Climate Change (IPCC) (2000), *Special Report on Emissions Scenarios: A Special Report of Working Group III of the Intergovernmental Panel on Climate Change*, 599 pp., Cambridge Univ. Press, Cambridge, U. K.

- Lindzen, R. S. (1981), Turbulence and stress owing to gravity wave and tidal breakdown, *J. Geophys. Res.*, *86*, 9707–9714, doi:10.1029/JC086iC10p09707.
- McFarlane, N. A. (1987), The effect of orographically excited gravity wave drag on the general circulation of the lower stratosphere and troposphere, *J. Atmos. Sci.*, *44*, 1775–1800.
- McLandress, C., and T. G. Shepherd (2009), Simulated anthropogenic changes in the Brewer-Dobson circulation, including its extension to high latitudes, *J. Clim.*, *22*, 1516–1540, doi:10.1175/2008JCLI2979.1.
- Palmer, T. N., G. J. Shutts, and R. Swinbank (1986), Alleviation of a systematic bias in general-circulation and numerical weather prediction models through an orographic gravity-wave drag parameterization, *Q. J. R. Meteorol. Soc.*, *112*, 1001–1039.
- Plumb, R. A. (2002), Stratospheric transport, *J. Meteorol. Soc. Jpn.*, *80*, 793–809.
- Rosenlof, K. H. (1995), Seasonal cycle of the residual mean meridional circulation in the stratosphere, *J. Geophys. Res.*, *100*, 5173–5191, doi:10.1029/94JD03122.
- Shepherd, T. G. (2007), Transport in the middle atmosphere, *J. Meteorol. Soc. Jpn.*, *85B*, 165–191.
- Son, S., L. M. Polvani, D. W. Waugh, T. Birner, H. Akiyoshi, R. R. Garcia, A. Gettelman, D. A. Plummer, and E. Rozanov (2009), The impact of stratospheric ozone recovery on tropopause height trends, *J. Clim.*, *22*, 429–445, doi:10.1175/2008JCLI2215.1.
- World Meteorological Organization/United Nations Environment Programme (WMO/UNEP) (2003), *Scientific Assessment of Ozone Depletion: 2002*, Nairobi.
-
- H. Akiyoshi, National Institute for Environmental Studies, 16-2 Onogawa, Tsukuba, Ibaraki 305-8506, Japan.
- K. Okamoto and K. Sato, Department of Earth and Planetary Physics, University of Tokyo, Tokyo 113-0033, Japan. (kota0@eps.s.u-tokyo.ac.jp)